Experimental Study of Frequency Control of LaSMP Laminated Beams

Huiyu Li
StrucTronics & Control Lab,
College of Aerospace Engineering,
Nanjing University of Aeronautics
and Astronautics,
Nanjing 211100, China
e-mail: dahuadvr@126.com

Dan Wang
StrucTronics & Control Lab,
College of Aerospace Engineering,
Nanjing University of Aeronautics
and Astronautics,
Nanjing 211100, China
e-mail: wangd12@nuaa.edu.cn

Hornsen Tzou[1]
Key Laboratory of Mechanics and Control
of Mechanical Structures;
StrucTronics & Control Lab; Interdisciplinary
Research Institute;
College of Aerospace Engineering,
Nanjing University of Aeronautics
and Astronautics,
Nanjing 211100, China
e-mail: hstzou@nuaa.edu.cn

Light-activated shape memory polymers (LaSMPs) exhibit stiffness variations when exposed to ultraviolet (UV) lights. Thus, LaSMP could manipulate structural frequencies with UV light exposures when laminated on structures. This study aims to experimentally demonstrate the effectiveness of LaSMP frequency control of a flexible beam. The natural frequency of a three-layered Euler–Bernoulli beam composed of LaSMP, adhesive tape, and the flexible beam is analyzed and its frequency formulation exhibits the LaSMP stiffness influence. Since the LaSMP adopted in this study is a new spiropyran-based composition—Sp3/EVA_4, a generic Young's modulus model is proposed and then simplified to model this new LaSMP composition. To guarantee a homogenous light field, light intensities on the UV surface light source at different positions are tested. The temperature change of the LaSMP sample under UV exposures is also measured. The time constant and the threshold intensity of the reverse reaction are measured. LaSMP Young's modulus variation is tested with a uniaxial tension experiment. The constitutive model of LaSMP's Young's modulus is validated by experimental data. With these preparations, the LaSMP laminated flexible beam model is exposed to UV lights and its natural frequencies are identified with data acquisition and analysis system. Then, natural frequency variations of 25%, 50%, 75%, to 100% exposure areas are also evaluated. The maximum natural frequency variation ratio achieves 9.7%; theoretical predictions and experimental data of LaSMP natural frequency control are compared very well. [DOI: 10.1115/1.4054436]

Keywords: LaSMP, cantilever beam, dynamic stiffness, frequency control, smart materials and structures, structural dynamics and control, vibration control

Introduction

Natural frequency and damping controls are the two essential vibration control techniques for engineering structures and systems. With smart materials, such as piezo-/flexo-electric, electro-/magneto-/photos-strictive, electro-/magnetorheological, and shape memory materials, active and "smart" distributed control systems can be realized [1–10]. These smart structures and structronic systems exhibit advantages of high integration and adaptivity in active precision actuation and vibration controls. Vibration control and precision actuations with various smart materials and structures have been extensively studied over the last three decades. Piezoelectric materials used as sensors and actuators were applied to the control of beams, plates, rings, and cylindrical shells [1,6]. Vibration control of hemispherical shells with light-activated shape memory polymers was evaluated [5,8]. With a response time of only milliseconds, magnetorheological (MR) materials were adopted to design controllable-stiffness components. With the current control, stiffness and damping ratio were enhanced by tens of percent [9]. Shape memory alloy (SMA) was also used to control the natural frequencies of a clamped-clamped beam and its natural frequency increases as the temperature rises [10]. A new light-activated shape memory polymer (LaSMP) also exhibits the dynamic stiffness effect when exposed to lights [11]. Compared with SMA, the LaSMP has the advantage of non-contact actuation and control, working at room temperature, low density, and cost [12].

LaSMP contains photo-sensitive ingredients; thus, chemical reactions occur under light exposures [13]. The LaSMP synthesized with cinnamate groups exhibits shape memory behavior with ultraviolet (UV) light exposures of two wavelengths. However, its response time takes about one hour [14,15]. The response time of LaSMP was significantly shortened to tens of seconds with the formulations based on azobenzene and spiropyran [16,17]. The LaSMP dynamic stiffness features were tested through uniaxial tensions. Lab experiments show LaSMP's modulus can cyclically change under ultraviolet exposures [16,18]. Thus, applications of LaSMP in design of smart structures become promising. Natural frequency controls of LaSMP laminated beams and shells were evaluated theoretically, and a second-order model of LaSMP's modulus based on chemical kinetics of a cinnamate-based LaSMP was presented [19]. LaSMP was also adopted to the dynamic vibration control of rings; the nonlinear behavior of LaSMP's modulus was improved by the phase shift and neural network control methods [20]. The methods of modeling LaSMP deformations include the chemical kinetics [18], the multi-natural configuration [21], the viscoplasticity [22], etc. Recently, a constitutive model of LaSMP based on the multi-natural configuration is established to represent the LaSMP deformation with inhomogeneous light exposures [23]. Among these models, the one based on chemical kinetics is relatively simple and practical in engineering applications [19].

In this study, a generic *k*th-order LaSMP constitutive model based on the chemical kinetics is established and simplified to a *new* spiropyran-based LaSMP formula (Sp3/EVA_4) synthesized in the StrucTronics and Control Lab. (at Zhejiang University). Material syntheses, characterization, and parameter identification of the new material are carried out first. The uniaxial tension test of LaSMP is conducted; LaSMP material parameters are measured and identified. The natural frequency variation of an LaSMP cantilever beam exposed to various UV lights is tested. Experimental data are compared with analytical results derived from the chemical kinetics model.

[1]Corresponding author.

Contributed by the Technical Committee on Vibration and Sound of ASME for publication in the Journal of Vibration and Acoustics. Manuscript received August 14, 2021; final manuscript received April 20, 2022; published online May 13, 2022. Assoc. Editor: Miao Yu.

Mathematical Models

Based on the study of flexible beams and shells laminated with LaSMP layers, the LaSMP is effective to manipulate structural frequencies when LaSMP is exposed to UV lights [19]. The LaSMP used in a previous study [20] and that in the current study are based on different material formulae or compositions. The one used in earlier studies is based on the photo-crosslinking cinnamate [19,20], and that synthesized in this study is based on the photo-isomerization spiropyran, reported in detail later. Accordingly, a more generalized LaSMP modulus model needs to be established. In this section, the LaSMP laminated beam model is briefly reviewed first. A generic kth-order LaSMP Young's modulus model, including both the forward and reverse reactions and its simplifications to the current material model, is presented next. LaSMP modulus control or controllable stiffness of the reverse and forward reactions is also defined. Synthesis of spiropyran-based LaSMP, material characterization, parameter identification, and a physical model and its laboratory experiments are presented later.

LaSMP Laminated Beam. As shown in Fig. 1, a flexible beam is bonded with a layer of LaSMP through a double-sided bonding tape. Since natural frequency control of this three-layer composite beam model with a newly synthesized LaSMP is evaluated in lab experiments later, its theoretical model and modal analysis are briefly reviewed. As both the flexible beam and the LaSMP layer are thin, the influence of double-sided bonding tape cannot be neglected. Thus, the three-layer LaSMP laminated beam is treated as a composite Euler–Bernoulli beam and its modal characteristics are briefly discussed.

The unit-width dynamic equation of the three-layered Euler–Bernoulli beam is expressed as [1,19]

$$\frac{1}{3}\sum_{i=1}^{3} Y_i(r_{i+1}^3 - r_i^3)\frac{\partial^4 u_3}{\partial x^4} + \sum_{i=1}^{3}\rho_i(r_{i+1} - r_i)\ddot{u}_3 = F_3 \tag{1}$$

where i is the layer number and $i = 1,2,3$, respectively, denoting the LaSMP layer, the adhesive and the flexible beam; Y_i is Young's modulus and ρ_i ($i = 1,2,3$) is the mass density per unit length of the ith layer; r_{i+1} and r_i ($i = 1,2,3$) is the distance from the modulus-weighted neutral surface to the bottom and top surfaces of the ith layer (Fig. 2). u_3 and F_3, respectively, denote the transverse displacement and the transverse excitation/unit width. Note that UV manipulations of LaSMP's Young's modulus Y_1 (the first layer) to the beam's natural frequency ω_m are focused and are compared with experimental results.

It is noted that $h_i = r_{i+1} - r_i$, and h_i is the ith layer thickness. u_3 and $\ddot{u}_3$ are the displacement and acceleration components in the transverse direction, and F_3 is the transverse external excitation per unit length. For a three-layered beam, the modulus-weighted

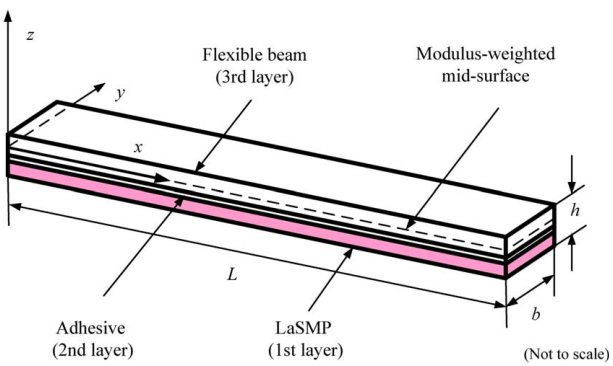

Fig. 1 A three-layer LaSMP laminated flexible beam

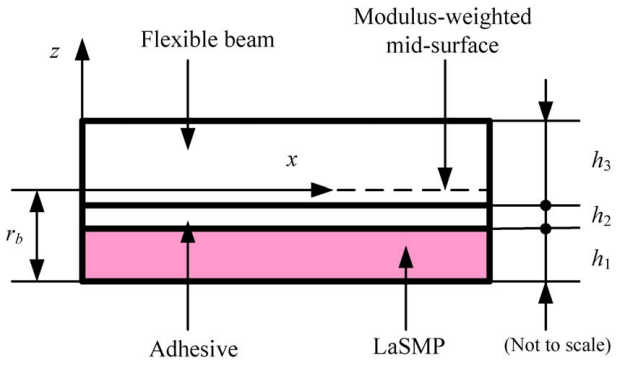

Fig. 2 Cross section of the LaSMP laminated beam

neural surface (axis) is given through a standard moment analysis [1]

$$r_b = \frac{Y_1 h_1^2 + Y_2(h_2^2 + 2h_1h_2) + Y_3(h_3^2 + 2h_1h_3 + 2h_2h_3)}{2(Y_1h_1 + Y_2h_2 + Y_3h_3)} \tag{2}$$

where r_b is the distance from the modulus-weighted mid-surface to the bottom of the laminated beam. Note that the coordinate axes are set referencing to the modulus-weighted mid-surface. In the experimental model presented later, the LaSMP is fully distributed on the flexible cantilever beam and partial exposures are regulated by a mask.

The beam natural frequency can be determined by the free vibration analysis. With the fixed-free boundary conditions, the modal shape function $U_3(x)$ is

$$U_{3m}(x) = \cosh\frac{\lambda_m}{L}x - \cos\frac{\lambda_m}{L}x - \frac{\sinh\lambda_m - \sin\lambda_m}{\cosh\lambda_m + \cos\lambda_m} \times \left(\sinh\frac{\lambda_m}{L}x - \sin\frac{\lambda_m}{L}x\right) \tag{3}$$

where m is the mode number; L is the beam length; λ_m is the eigenvalue

$$\lambda_m^4 = \frac{\sum_{i=1}^{3}\rho_i(r_{i+1} - r_i)}{\frac{1}{3}\sum_{i=1}^{3} Y_i(r_{i+1}^3 - r_i^3)}\omega_m^2 \tag{4}$$

and $\lambda_1 L = 1.875$, $\lambda_2 L = 4.694$, $\lambda_3 L = 7.855\ldots$ for mode $m = 1,2,3..$, The natural frequency ω_m (rad/s) of the LaSMP laminated composite beam becomes

$$\omega_m = \frac{(\lambda_m L)^2}{L^2}\sqrt{\frac{1}{3}\sum_{i=1}^{3} Y_i(r_{i+1}^3 - r_i^3)\Big/\sum_{i=1}^{3}\rho_i(r_{i+1} - r_i)} \tag{5}$$

Note that the influence of LaSMP's Young's modulus Y_1 (the first layer) on the natural frequency ω_m is embedded in Eq. (5). When the whole laminated beam is under light exposures, variation of natural frequencies can be evaluated accordingly. The range of natural frequency variation can also be manipulated by restricting the LaSMP exposed area realized by setting a mask above the LaSMP layer (Fig. 3). Thus, only a part of the LaSMP layer is exposed, and only its local Young's modulus is changed.

During the lab experiments, the effect of mask exposures is also evaluated. The LaSMP is still fully distributed on the surface of the flexible beam, and the area under exposure is restricted from the clamped end $x = 0$ to an arbitrary point $x = x^*(0 < x^* < L)$ (Fig. 3). For the mask exposure, the LaSMP laminated beam can be assumed as a stepped beam [19]. The first section denotes the area under exposure, and the second section represents the area under a mask. Although the cross-sections of the first section and the second section are the same, Young's modulus of the first

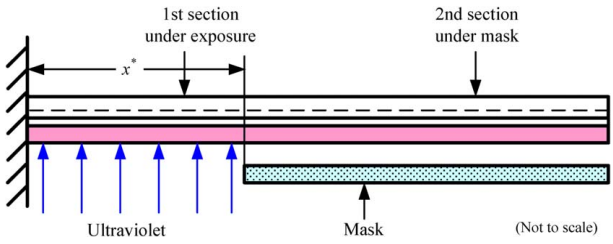

Fig. 3 The LaSMP laminated beam with mask exposures

section varies under light exposures and that of the second section remains unchanged with the mask. The displacement, slope, moment, and shear force should be continuous between the first and second sections.

Recall that the newly synthesized LaSMP in this study and that in the previous study are different formulations [19] and their Young's modulus variations exhibit opposite behaviors. As the new spiropyran-based LaSMP used in the experiment changes from a hard state to a soft state under the UV exposures, the initial LaSMP Young's modulus before exposure is assumed to be $Y_{\max}$. Thus, the boundary condition at $x = x^*(0 < x^* < L)$ at the effective LaSMP length (Fig. 3) is expressed as

$$[u_3(x^*)]_1 = [u_3(x^*)]_2, \qquad \frac{\partial[u_3(x^*)]_1}{\partial x} = \frac{\partial[u_3(x^*)]_2}{\partial x} \tag{6a,b}$$

$$\frac{1}{3}\sum_{k=1}^{3} Y_k(r_{k+1}^3 - r_k^3)\frac{\partial^2[u_3(x^*)]_1}{\partial x^2} = \frac{1}{3}[Y_{\max}(r_2^3 - r_1^3) + Y_2(r_3^3 - r_2^3) + Y_3(r_4^3 - r_3^3)]\frac{\partial^2[u_3(x^*)]_2}{\partial x^2} \tag{7}$$

$$\frac{1}{3}\sum_{k=1}^{3} Y_k(r_{k+1}^3 - r_k^3)\frac{\partial^3[u_3(x^*)]_1}{\partial x^3} = \frac{1}{3}[Y_{\max}(r_2^3 - r_1^3) + Y_2(r_3^3 - r_2^3) + Y_3(r_4^3 - r_3^3)]\frac{\partial^3[u_3(x^*)]_2}{\partial x^3}, \tag{8}$$

where $[u_3(x^*)]_1$ denotes the transverse displacement of the first section and $[u_3(x^*)]_2$ denotes the transverse displacement of the second section. The boundary conditions of the clamped end ($x = 0$) and the free end ($x = L$) remain unchanged. Again, with the free vibration analysis, the natural frequency of the cantilever beam under mask exposures could be studied and the partial exposure effects can be evaluated. To analyze the influence of LaSMP on the flexible beam, Young's modulus of the newly synthesized LaSMP is modeled next. Material characterizations and parameter identification are carried out in the first part of lab experiments, followed by frequency control of the laminated beam with UV light irradiations.

LaSMP Young's Modulus Control. The LaSMP contains optically activated species whose concentration P changes under UV exposures. Phenomenally, LaSMP alternates between the hard state and the soft state. The general model of LaSMP's modulus was established based on the chemical kinetics [20]. For different LaSMP compositions, the reaction order could also change, and thus, a generic kth-order model needs to be established first. The LaSMP used in this study is lab proved to be the first order (presented later); accordingly, the generic model needs to accommodate the first-order behavior and be validated in lab experiments.

The generic LaSMP model describes two reversible processes: *the forward reaction* and *the reverse reaction*. In the forward reaction, the concentration of optically activated species increases and LaSMP changes from the *soft* state to the *hard* state; in the reverse reaction, the concentration of optically activated species decreases and LaSMP goes back to the soft state. Note again that the LaSMP adopted in this study is set in the free-strain condition. It changes from the hard state to the soft state under UV light exposures. Thus, the reverse reaction happens first and the forward reaction happens subsequently as the UV light being turned on/off on the newly synthesized LaSMP. For this reason, here LaSMP's reverse reaction model is described before the forward reaction model.

(1) Reverse reaction

The reverse reaction starts as the UV light is turned *on*. Before the UV exposure, the concentration of optically activated species P remains at the maximum, i.e., $P_{\max}$. It reduces to zero if the exposure time goes to infinity. The generic kth-order concentration model of the reverse reaction is expressed as [20]

$$\tau_d \frac{dP}{dt} + P^k = 0 \tag{9}$$

where τ_d is the time constant of the reverse reaction and k is the reaction order. The LaSMP used here follows the first order, i.e., $k = 1$, and the concentration equation is simplified to

$$\tau_d \frac{dP}{dt} + P = 0 \tag{10}$$

The time constant τ_d is defined as

$$\tau_d = \left[k_d \frac{(I_d)_{\text{avg}} - (I_d)_{\text{th}}}{(I_d)_{\text{th}}}\right]^{-1} \tag{11}$$

where k_d is the material constant of the reverse reaction; $(I_d)_{\text{avg}}$ is the averaged light intensity, and $(I_d)_{\text{th}}$ is the threshold intensity in the reverse reaction. If the UV light intensity is lower than the threshold intensity $(I_d)_{\text{th}}$, the reverse reaction does not start and Young's modulus remains unchanged. The UV light strength is proportional to the thickness direction of the LaSMP layer. According to the Beer–Lambert–Bouguer Law, the light intensity decays exponentially in LaSMP sample [24]

$$I_d(\alpha_3, t) = I_d(t)e^{-c_d\alpha_3} \tag{12}$$

where α_3 represents the thickness direction; $I_d(\alpha_3,t)$ is the α_3 light intensity in the reverse reaction; $I_d(t)$ is the light intensity on the incident surface, and c_d is the attenuation coefficient in the reverse reaction. The averaged light intensity $(I_d)_{\text{avg}}$ in the reverse reaction is obtained by integrating the light intensity $I_d(\alpha_3,t)$ and averaging in the LaSMP thickness

$$(I_d)_{\text{avg}} = \frac{1}{h_1}\int_0^{h_1} I_d(t)e^{-c_d\alpha_3}d\alpha_3 = \frac{I_d(t)}{c_d h_1}(1 - e^{-c_d h_1}) \tag{13}$$

Note that h_1 is the LaSMP thickness. With an initial concentration $P = P_{\max}$, the concentration P of optically activated species in the reverse reaction of the first-order model (Eq. (10)) is solved and the concentration behaves as

$$P = P_{\max}e^{\frac{-t}{\tau_d}} \tag{14}$$

Assuming the duration of UV exposure is t_1, the concentration of optically activated species is $P_{t_1} = P_{\max}e^{\frac{-t_1}{\tau_d}}$ at the end of the reverse reaction. This concentration is taken as the initial condition of the forward reaction.

(2) Forward reaction

The forward reaction begins as the UV light is turned *off*. The generic kth-order forward reaction model is expressed as

$$\tau_r \frac{dP}{dt} - (P_{\max} - P)^k = 0 \tag{15}$$

Again, for the newly synthesized LaSMP here, the reaction order $k = 1$. Thus, the first-order forward reaction becomes

$$\tau_r \frac{dP}{dt} + P = P_{\max} \tag{16}$$

where τ_r is the time constant of the forward reaction. It is defined as

$$\tau_r = \left[k_r \frac{(I_r)_{\text{avg}} - (I_r)_{\text{th}}}{(I_r)_{\text{th}}} \right]^{-1} \tag{17}$$

where k_r is the material constant of the forward reaction; $(I_r)_{\text{avg}}$ and $(I_r)_{\text{th}}$ are the averaged light intensity and the threshold intensity in the forward reaction, respectively. Accordingly, the light intensity in the forward reaction is expressed as

$$I_r(\alpha_3, t) = I_r(t) e^{-c_r \alpha_3} \tag{18}$$

where $I_r(\alpha_3,t)$ and $I_r(t)$ are the light intensity and the light intensity on the LaSMP incident surface in the forward reaction, respectively; c_r is the attenuation coefficient in the forward reaction. The averaged light intensity in the forward reaction $(I_r)_{\text{avg}}$ is expressed as

$$(I_r)_{\text{avg}} = \int_0^{h_1} I_r(t) e^{-c_r \alpha_3} d\alpha_3 / h_1 = I_r(t)(1 - e^{-c_r h_1})/c_r h_1 \tag{19}$$

Recall that the initial condition of the forward reaction is $P_{t_1} = P_{\max} e^{\frac{-t_1}{\tau_d}}$. The concentration P of optically activated species in the forward reaction (Eq. (16)) is solved and the concentration becomes

$$P = P_{\max} - P_{\max} e^{\frac{-t}{\tau_r}} + P_{\max} e^{\frac{-t_1}{\tau_d} + \frac{-t}{\tau_r}} \tag{20}$$

LaSMP Modulus Control. Recall that the top layer of the laminated beam model is the LaSMP layer denoted as the first layer. LaSMP Young's modulus Y_1 is assumed to be proportional to the concentration P of optically activated species [20]. Thus, Y_1 is expressed as

$$Y_1 = Y_{\min} + (Y_{\max} - Y_{\min}) P / P_{\max} \tag{21}$$

where $Y_{\min}$ is the minimum Young's modulus when the UV exposure time goes to infinity. Recall that $Y_{\max}$ is the maximum Young's modulus of the LaSMP before UV exposure and it is determined by the uniaxial tension experiment. Substituting Eqs. (14) and (20) into Eq. (21) yields the UV-controlled moduli in the reverse reaction and the forward reaction of the first-order model, respectively

$$\text{(1) Reverse reaction: } Y_1 = Y_{\min} + (Y_{\max} - Y_{\min}) e^{\frac{-t}{\tau_d}} \tag{22}$$

$$\text{(2) Forward reaction: } Y_1 = Y_{\min} + (Y_{\max} - Y_{\min}) \left(1 - e^{\frac{-t}{\tau_r}} + e^{\frac{-t_1}{\tau_d} + \frac{-t}{\tau_r}} \right) \tag{23}$$

Accordingly, with the controllable LaSMP's Young's modulus, variation of the natural frequency can be analyzed. Next, in lab experiments, the attenuation coefficient c_d is measured first; then, the uniaxial tension of LaSMP sample is carried out to validate the first-order model. The threshold intensity $(I_d)_{\text{th}}$ in the reverse reaction is further evaluated; the natural frequency of LaSMP laminated beam under laser exposures is measured, evaluated, and compared last.

LaSMP Characterization and Parameter Identification

In this section, the LaSMP's modulus model is validated by experiments. Preparation of LaSMP samples in the StrucTronics and Control Lab is briefly introduced. To carry out various material characterization and vibration control experiments, there are three different LaSMP samples cut off from the same lab-made patch, which are used in four experiments. In the first experiment, the attenuation coefficient of a square layer (Sample-1: 20 mm × 20 mm × 0.1 mm) in the reverse reaction c_d is determined; in the second experiment, Young's modulus variation of an LaSMP strip (Sample-2: 120 mm × 10 mm × 0.18 mm) under UV exposures is tested through uniaxial tension tests; in the third experiment, the threshold intensity in the reverse reaction $(I_d)_{\text{th}}$ is measured; and in the fourth experiment, natural frequency variations of the LaSMP laminated beam with full and partial UV exposures are tested. Note that the third and fourth experiments are based on an LaSMP laminated beam (Sample-3: 80 mm × 6 mm × 0.43 mm). All were taken from the same LaSMP batch. Since the first and second experiments are related to material characterization and parameter identifications, they are grouped in this section. The third and fourth experiments are based on the same lab setup; they are grouped in the next section. Finally, the theoretical natural frequency results of the LaSMP laminated beam are compared with experimental data.

Synthesis of LaSMP (Sp3/EVA_4). The LaSMPs are composed of spiropyran and ethylene-vinyl acetate copolymers (EVA) [16]. The molecular formula of spiropyran is 3′, 3′-Dimethyl -1′-(2-hydroxyethyl) -6- nitrospiro [2H-1- benzopyran-2, 2′- indoline]. The concentration of spiropyran in the LaSMP is 3%. The EVA is E180F manufactured by Samsung. Both the spiropyran and EVA are dissolved in toluene (a liquid aromatic hydrocarbon C7H8) in the StrucTronics and Control Lab. Then, the solution is poured into a glass mold. The mold with the solution is put in a constant temperature oven to dry. The temperature remained at 70 °C for 2 h. The raw LaSMP films are acquired after the toluene evaporated. To acquire LaSMP films with uniform thickness, the raw LaSMP films are further processed by two vulcanizing machines. Finally, the LaSMP films are cut into specific shapes or samples used for lab experiments and the laminated beam model.

Attenuation Coefficient Measurement. The attenuation coefficient c_d in the reverse reaction is an important parameter as it reflects the UV absorbing ability of LaSMP. An LaSMP film with a thickness of 0.1 mm is tested. Both the length and width of the LaSMP sample are 20 mm, i.e., Sample-1: 20 mm × 20 mm × 0.1 mm. A UV surface light source (Lamplic Technology, UVEC8-72A, Shenzhen, China) with an effective light area of 100 mm × 100 mm is employed for the experiment. The central wavelength of the surface UV source is 365 nm. A UV light meter (Kühnast Radiation GmbH, KUHNAST UV-365A, Germany) is used to measure the UV light intensity. The LaSMP film is put in the UV light field. Then, the light intensity on the incident surface and the exit surface are picked up, respectively. The light intensity on the incident surface is 39.375 mW/cm^2, and on the exit surface is 1.555 mW/cm^2. With the Beer–Lambert–Bouguer law in Eq. (18), the light intensity in the LaSMP thickness direction decreases exponentially. The attenuation coefficient in the reverse reaction c_d is determined by substituting the measured light intensities into Eq. (16). As the light intensity keeps constant in the experiment, i.e., on the incident surface $\alpha_3 = 0$ mm, $I_d(t)$ is always equal to 39.375 mW/cm^2. On the exit surface $\alpha_3 = 0.1$ mm, $I_d(a_3, t)|_{\alpha_3=0.1} = 1.555$ mW/cm^2. c_d is solved by substituting these terms into Eq. (18)

$$I_d(a_3, t)|_{\alpha_3=0.1} = 39.375 e^{-c_d * 0.1} \text{ mW/cm}^2 \tag{24}$$

Thus, the attenuation coefficient in the reverse reaction c_d is determined as 32.32. It is useful to determine the averaged light intensity $(I_d)_{\text{avg}}$. The distribution of UV light intensity in the LaSMP thickness is plotted in Fig. 4.

Uniaxial Tension Experiment. The uniaxial tension test is a general method to gain the stress–strain relationship of film materials [25]. An LaSMP strip (Sample-2: 120 mm × 10 mm × 0.18 mm) is prepared according to the testing standard: GB/T 1040.3-2006/

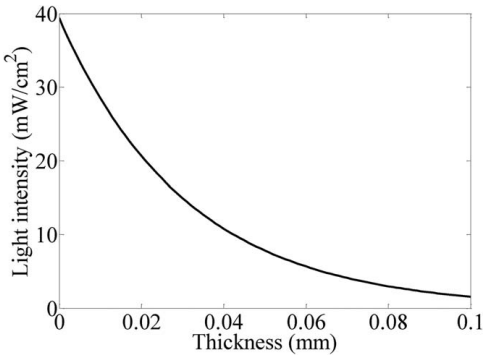

Fig. 4 Distribution of UV light intensity through the LaSMP sample

ISO 527-3:1995 [26]. It defines the test conditions for films and sheets when measuring their tensile properties. In lab experiments, a uniaxial tension instrument specially designed for testing soft films is employed. The maximum tensile force is 50 N. The resolution of force is 0.1 N, and the resolution of displacement is 1 μm. The tension speed ranges from 10 mm/min to 200 mm/min.

Since defects on the sample boundaries greatly influence its performance. The LaSMP film is cut by a surgical knife. The LaSMP samples (Sp3/EVA_4) are cut into a dimension as 120 mm(length) × 10 mm(width) (Fig. 5). The thickness is measured from randomly selected five positions of a sample and averaged. The averaged thickness is 0.18 mm. The length of the two clamped ends is 3 0mm; thus, the length of the samples under exposure is 90 mm.

As the existence of stress relaxation and creep, Young's moduli of soft films are not constant with respect to different tension speeds. Thus, the strain–stress curves under various tension speeds are tested and shown in Fig. 6, and the tests are done without UV light exposures.

It is noted that the strain–stress curves under 10 mm/min and 20 mm/min are similar. As the tension speeds are low, and one tension cycle lasts for more than 30 s, the stress relaxation is obvious. For the relatively high tension speeds 50 mm/min, 100 mm/min and 200 mm/min, the slopes of the stress–strain curves are relatively stable. The stress relaxation is not apparent. Young's moduli obtained by curve fitting are 41.28 MPa, 40.54 Mpa, and 41.09 Mpa for the tension speeds 50 mm/min, 100 mm/min, and 200 mm/min, respectively. Besides, for the natural frequency control, the response time of LaSMP is shorter the better. As Young's moduli with the tension speed above 50 mm/min are stable, the tension speed is set at 50 mm/min in the following uniaxal tension experiment with UV exposures.

Fig. 5 The LaSMP samples (Sp3/EVA_4) for the uniaxial tension experiment

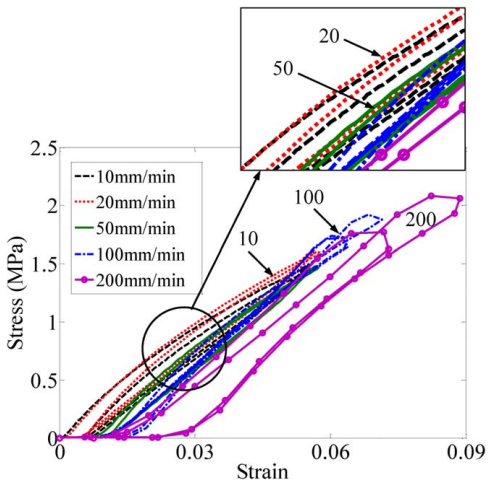

Fig. 6 LaSMP behaviors under different tension speeds

Before starting the experiment, the light intensity is measured to ensure the LaSMP sample is put in a homogeneous light field. The UV light intensity is measured at the randomly selected five positions along the length direction of LaSMP samples (Sp3/EVA_4). The measured light intensities are 40.625 mW/cm^2, 40.500 mW/cm^2, 40.473 mW/cm^2, 40.260 mW/cm^2 and 40.165 mW/cm^2 respectively. The averaged UV light intensity is 40.405 mW/cm^2. It shows that the light field is homogenous and the UV surface light source can be used in exposure experiments.

After these preparations, the uniaxial tension of the LaSMP sample under UV exposures is carried out. The stress–strain curves are shown in Fig. 7. It is noted that each cycle is composed of the loading and unloading processes.

Uniaxial tension test cycle-1 is completed before the UV exposure is turned on, and it is used to determine the initial Young's modulus Y_{max} before UV exposures. From cycle-2 to cycle-5, the UV light keeps exposure. Then, the UV light is turned off for cycle-6 to cycle-10. Young's modulus in each cycle is obtained by fitting each loading curve. The results are given in Fig. 8. It is obvious that Young's modulus of LaSMP decreases when UV light is *on* and increases when UV light is *off*. Thus, the initial Young's modulus Y_{max} before UV exposures is obtained as 42.1 MPa. After being exposed for 36 s, Young's modulus in cycle-5 is reduced to 20.29 MPa. When the UV light is turned off at 42.4 s, i.e., the time in the experiment is 78.4 s, Young's modulus of cycle-10 recovers to 38.42 MPa. This test shows that LaSMP Young's modulus under UV exposures changes by 51.8% and Young's modulus recovery percentage is 91.3% at the time of 78.4 s. The experiment data suggest that the dynamic stiffness feature of LaSMP is promising for the application in frequency control.

With the established Young's modulus mathematical model in Eqs. (22) and (23), Young's moduli from the first-order chemical kinetics model are also illustrated in Fig. 8 and compared with the experiment data. It is noted that the maximum Young's modulus Y_{max} in the model is determined by the uniaxial tension experiment cycle-1. The maximum concentration of optically activated species P_{max} is determined by the LaSMP composition. Results of the chemical kinetics model show that the initial Young's modulus of LaSMP is 42.1 MPa. After the UV light

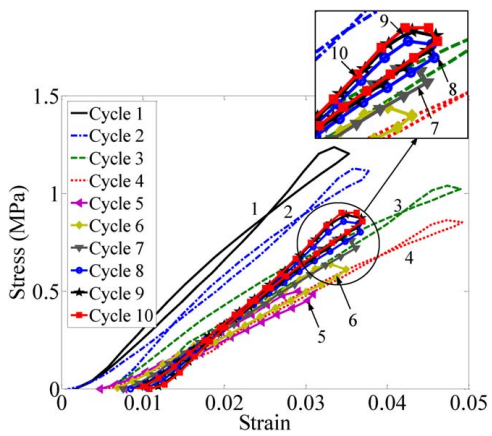

Fig. 7 Uniaxial tension tests of LaSMP sample (Sp3/EVA_4)

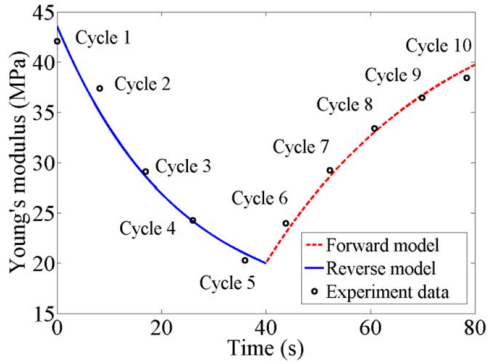

Fig. 8 Young's moduli data from the chemical kinetics model and the uniaxial tension test (lines: theory; dots: experiment)

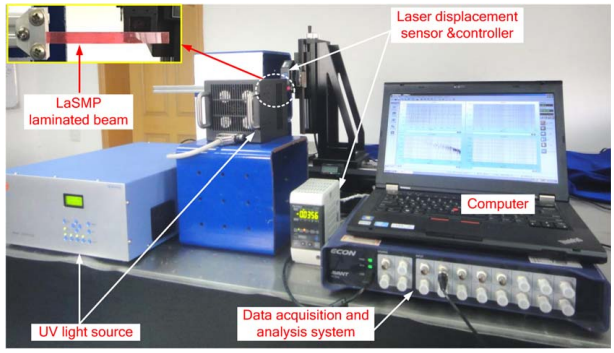

Fig. 9 Lab setup of the natural frequency control of an LaSMP laminated beam

exposure for 40 s, LaSMP Young's modulus reduces to 20.19 MPa. After the UV light is turned off for another 40 s, LaSMP Young's modulus recovers to 38.5 MPa. The root-mean-square error (RMSE) of the reverse model is 1.756 MPa, and the RMSE of the forward model is 1.004 MPa. Thus, the first-order Young's modulus model describes the LaSMP behavior under UV exposures very well, and the theoretical model is validated by the laboratory experiments.

In lab prepared samples (Sp3/EVA_4), the spiropyran concentration in the LaSMP sample is 3%. Other parameters such as the minimum Young's modulus $Y_{\min}$, the time of reverse reaction t_1, time constants τ_r, and τ_d are determined in the curve fitting processes based on lab experimental data. All essential parameters are summarized in Table 1.

Recall that the definition of the time constant of the reverse reaction τ_d in Eq. (11): τ_d is related to the material constant of the reverse reaction k_d, the averaged light intensity $(I_d)_{\text{avg}}$, and the threshold intensity in the reverse reaction $(I_d)_{\text{th}}$. Once the parameters of τ_d, $(I_d)_{\text{avg}}$, and $(I_d)_{\text{th}}$ are known, the material constant of the reverse reaction k_d could be determined. $(I_d)_{\text{avg}}$ is calculated by substituting the known terms: the attenuation coefficient in the reverse reaction c_d, the light on the incident surface I_r, and the thickness of LaSMP h_1 into Eq. (13). The averaged light intensity in the uniaxial tension experiment is 6.925 mW/cm^2. As the threshold intensity in the reverse reaction $(I_d)_{\text{th}}$ is only related to the LaSMP composition and the wavelength of UV lights, it is tested in the next experiment: natural frequency control of LaSMP laminated beams. When $(I_d)_{\text{th}}$ is acquired, the material constant of the reverse reaction k_d can be obtained by Eq. (11).

Frequency Control of an LaSMP Laminated Beam

In this experiment, an LaSMP laminated beam is prepared and tested. The natural frequency of the beam is first acquired by the hammer excitation method. The experiment setup is displayed in Fig. 9. The LaSMP laminated beam is irradiated with UV light with a central wavelength of 365 nm. The transient displacement of the beam is measured by the laser displacement sensor (Keyence LK-G30) & controller (Keyence LK-GD500). Then, the displacement signal is input into the data acquisition and analysis system (DAS). The first natural frequency is evaluated through the DAS modal analysis module. The resolution of the laser displacement sensor (Keyence LK-G30) is 0.1 μm. The DAS sample frequency is set as 0.078 Hz.

Table 1 Parameters of the LaSMP chemical kinetic model

Parameters of LaSMP	Value
Reaction order k	1
Minimum Young's modulus, $Y_{\min}$	15 MPa
Maximum Young's modulus, $Y_{\max}$	42.1 MPa
Maximum concentration of optically activated species, $P_{\max}$	0.03
Time of the reverse reaction, t_1	40 s
Time constant of the forward reaction, τ_r	22.16
Time constant of the reverse reaction, τ_d	24.21
Light intensity on the incident surface, I_r	40.405 mW/cm^2
Thickness of LaSMP, h_1	0.18 mm

The LaSMP laminated beam sample is shown in Fig. 10. Its material properties and geometry parameters are listed in Table 2. The flexible beam is made of polypropylene (PP) film. The double-sided adhesive is 3M^{TM} VHB^{TM} F9460PC. Before starting the natural frequency test, the UV light intensity is also measured by randomly selected five positions along the beam length. To enhance the LaSMP response speed, the light intensity employed in the nature frequency control experiments is higher than that in the uniaxial tension experiments. The light intensities are 79.025 mW/cm^2, 78.354 mW/cm^2, 80.367 mW/cm^2, 80.794 mW/cm^2, and 80.520 mW/cm^2, respectively. Thus, the averaged light intensity in the incident surface of the LaSMP laminated beam is 79.812 mW/cm^2.

To identify that the natural frequency variation is actually caused by LaSMP Young's modulus changes, a single-layered PP beam is put in the same place of the light field, and its natural frequencies before and after UV exposures are also tested. The natural frequencies are tested five times, respectively. The averaged natural frequency of the first mode before UV exposures is 6.480 Hz. After being exposed to UV lights for 10 s, it changes to 6.375 Hz. Besides, the PP beam laminated with adhesive is also tested in the same way. The averaged natural frequency before UV exposure is 5.500 HZ, and after UV exposure for 10 s is 5.391 Hz. Thus, the UV light influence on the natural frequency of PP beam without

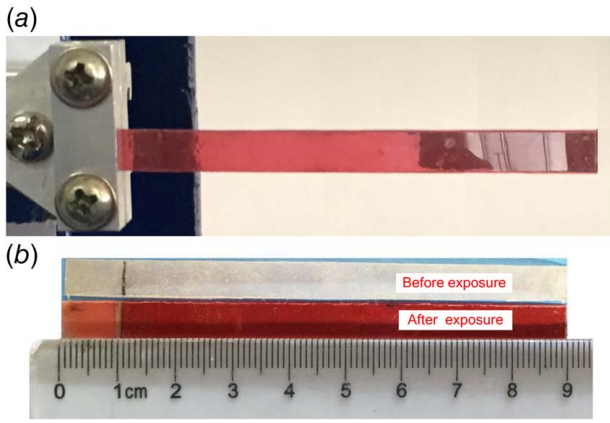

Fig. 10 LaSMP laminated beam: (*a*) cantilever beam and (*b*) beam before and after exposures of UV light

Table 2 Material properties and geometry of the LaSMP laminated beam

Property	Value
Young's modulus of the LaSMP, Y_1	20.19 ~ 42.1 MPa
Mass density of the LaSMP, ρ_1	950 kg/m^3
Thickness of the LaSMP, h_1	0.09×10^{-3} m
Young's modulus of the adhesive, Y_2	0.45 MPa
Mass density of the adhesive, ρ_2	980 kg/m^3
Thickness of the adhesive, h_2	0.05×10^{-3} m
Young's modulus of the flexible beam (PP), Y_3	1523 MPa
Mass density of the flexible beam (PP), ρ_3	946 kg/m^3
Thickness of the flexible beam (PP), h_3	0.19×10^{-3} m
Length of the LaSMP laminated beam, L	80×10^{-3} m
Width of the LaSMP laminated beam, b	6×10^{-3} m
Thickness of the LaSMP laminated beam, h	0.43×10^{-3} m

LaSMP is insignificant, and it is likely introduced by light-induced heat.

As LaSMP exhibits an advantage of working in room temperatures, the temperature influence of UV lights to the LaSMP laminated beam is also tested. A thermocouple is contacted with the incident surface of the LaSMP laminated beam. The full beam is under UV exposure, and the UV light exposure lasts for 10 s. The temperature of the LaSMP laminated beam before UV exposure is 19.3 °C, and after UV exposure is 26.3 °C. To enable the fast response of LaSMP, the light intensity is about ten times higher than the previously reported LaSMP experiments of (3 ~ 8 mW/cm^2) [14,27]; thus the variation of temperature is relatively obvious. While the light intensity decreases to 29.7 mW/cm^2, the temperature only increases 1.5 °C during the exposure of 10 s, from 20.1 °C to 21.6 °C. However, the nature frequency change is slow down at the same time. Thus, the light intensity is kept at 79.812 mW/cm^2 with an acceptable temperature variation of 7 °C in the following experiment.

Threshold Intensity Measurement. The threshold intensity $(I_d)_{\text{th}}$ in the reverse reaction needs to be measured to determine Young's modulus model, so the frequency calculation, is fully functional. The test is carried out with the same setup of natural frequency control experiments (Fig. 9). The distance between the UV light source and LaSMP laminated beam becomes separated. The light intensity is so low as no natural frequency variation happens to the LaSMP laminated beam. At this condition, the measured light intensity is 0.576 mW/cm^2. With these data and parameter measurements, frequency control experiments of the LaSMP laminated beam with UV (1) full exposures and (2) partial exposures can proceed next. Experimental data are compared with theoretical predictions later.

Frequency Control With Full LaSMP Ultraviolet Exposures. After these preparations, natural frequency control of the LaSMP laminated beam is proceeded. The natural frequency variations of the full LaSMP laminated beam under full exposures are presented in Fig. 11. The tests are repeated four times. The first natural frequency before UV exposure is 5.234 Hz. After exposure for 10 s, it reduces to 4.727 Hz—the reverse reaction, averaged by four experiments. Then, the natural frequency recovers to 5.234 Hz around about 100 s—the forward reaction. Note that the LaSMP Young's modulus recovers with the visible light of 540 ~ 560 nm. The experiment is carried out with no additional visible light source. Thus, the natural frequency recovery takes a longer time than that of the reducing process, which was also proved in the uniaxial tension experiment presented earlier. The natural frequency varies about 9.7% under UV exposures.

Frequency Control With Partial LaSMP Ultraviolet Exposures. To test the effect of partial LaSMP exposures, the exposure area is changed by putting a mask on the free end of the beam, shown in Fig. 3. The natural frequency variations with the exposure area of $L/4(25\%)$, $L/2(50\%)$, $3L/4(75\%)$, and $L(100\%)$ are plotted in Fig. 12. It is noted that the beam natural frequencies with exposure areas of $3L/4$ and L are almost the same. This is also validated by the theoretical predictions presented next.

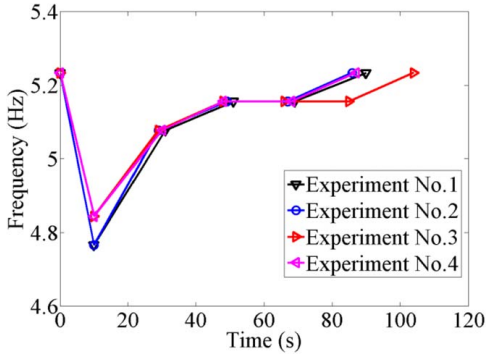

Fig. 11 Natural frequency variation of LaSMP laminated beam under full UV exposures

Comparison and Discussions

To validate the first-order LaSMP model, its theoretical calculations are compared with experimental data in this section. Substituting the threshold intensity $(I_d)_{\text{th}}$ and other parameters into Eq. (11) yields the material constant k_d of the reverse reaction. The averaged light intensity $(I_d)_{\text{avg}}$ in the reverse reaction is obtained with Eq. (13). With k_d, $(I_d)_{\text{avg}}$ and $(I_d)_{\text{th}}$, the time constant τ_d of the reverse reaction in the natural frequency control experiment can be determined. The LaSMP parameters used to determine Young's modulus variation are summarized in Table 3.

Young's modulus variation is obtained by substituting these parameters into Eq. (22). The results are: before the UV exposure, Young's modulus is 42.1 MPa, and after 10 s exposure, Young's modulus is 20.2 MPa. The two Young's moduli are used to infer and analyze the natural frequency variations of the LaSMP

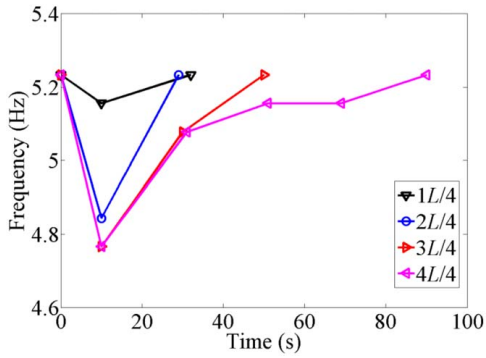

Fig. 12 Natural frequency variation of the LaSMP laminated beam under mask exposures

Table 3 Parameters of the first-order model

Parameters of LaSMP	Value
Attenuation coefficient in the reverse reaction, c_d	32.32
Material constant of the reverse reaction, k_d	3.7×10^{-3}
Threshold intensity, $(I_d)_{\text{th}}$	0.576 mW/cm^2
Light intensity on the incident surface, I_d	79.812 mW/cm^2
Averaged light intensity, $(I_d)_{\text{avg}}$	25.942 mW/cm^2
Time constant of the reverse reaction, τ_d	6.06

Table 4 Natural frequency of the LaSMP laminated beam before UV exposure

Math model (Hz)	Experiment (Hz)	Error (%)
4.953	5.234	5.67

Table 5 Natural frequencies of the laminated beam after mask UV exposures

Exposure area	$L/4$	$L/2$	$3L/4$	L
Math model (Hz)	4.828	4.785	4.777	4.776
Experiment (Hz)	5.156	4.844	4.688	4.688
Error (%)	6.79	1.23	−1.86	−1.84

laminated beam. With LaSMP Young's modulus of 42.1 MPa before UV exposure, the first natural frequency of the laminated beam before UV exposure is estimated by Eq. (5). Both theoretical and experimental results are listed in Table 4.

The error between the theoretical model calculation and the lab data is 5.67%. With LaSMP Young's modulus after UV exposure of 10 s is 20.2 MPa, the natural frequencies of the laminated beam after UV exposures are evaluated with two different conditions: (1) full LaSMP exposure and (2) partial LaSMP exposures. The result of full area exposure is also given in Eq. (5). The results of partial area exposure, such as $L/4$, $L/2$ and $3L/4$, are analyzed by the stepped beam theory [19]. All these natural frequencies after UV exposures are summarized in Table 5, and the maximum error is 6.79%. From the comparison of the theoretical calculations and the experimental data, it is proved that the chemical kinetics model is capable of describing LaSMP Young's modulus variations. Experimental results are compared very well with the analytical predictions.

Conclusions

LaSMP exhibits the dynamic stiffness feature under the ultraviolet stimuli. It provides wireless non-contact control of structural frequencies. This study focused on laboratory experiments of material characterization of spiropyran-based LaSMPs (Sp3/EVA_4) and natural frequency control of an LaSMP laminated cantilever beam. Theoretical models of the LaSMP laminated beam and LaSMP Young's moduli (including the reverse and forward reactions) were presented first. The parameters defined in the LaSMP's modulus model were directly measured through lab experiments or determined based on experimental data, such as the time constant of the reverse reaction τ_d, the material constant of the reverse reaction k_d, the averaged light intensity $(I_d)_{\text{avg}}$, and the threshold intensity in the reverse reaction $(I_d)_{\text{th}}$. The uniaxial tension experiment was carried out to characterize the LaSMP dynamic stiffness. It was observed that the LaSMP's modulus changed from 42.1 Mpa to 20.19 Mpa during the UV exposures and recovered to 38.42 Mpa at the end of the uniaxial tension experiment. Natural frequency control of an LaSMP laminated beam with full and partial UV exposures was also carried out. The exposure area was changed from $L/4$ to L to study the effects of mask exposures. Experimental natural frequency variation was compared with that estimated from the LaSMP's modulus model [19] and the errors were under 6.79%. These experiments provide a procedure to characterize new LaSMP materials and also prove that LaSMP is promising in the application of frequency control of flexible structures.

Acknowledgment

This work was supported by the National Natural Science Foundation of China (Grant No. 11872206), and the Key Laboratory of Mechanics and Control of Mechanical Structures (Nanjing University of Aeronautics and astronautics) (Grant No. MCMS-I-0521G01). The research was carried out, in part, in the StrucTronics and Control Lab at Zhejiang University and partially presented at the ASME 2016 International Design Engineering Technical Conferences and Computers and Information in Engineering Conference, Charlotte, NC, USA, DETC2016-59818.

Conflict of Interest

There are no conflicts of interest.

References

[1] Tzou, H. S., 2019, *Piezoelectric Shells: Sensing, Energy Harvesting, and Distributed Control*, 2nd ed. ed., Springer-Nature, Dordrecht, The Netherlands..
[2] Tzou, H. S., Lee, H. J., and Arnold, S. M., 2004, "Smart Materials, Precision Sensors/Actuators, Smart Structures, and Structronic Systems," Mech. Adv. Mater. Struc., **11**(4–5), pp. 367–393.
[3] Tzou, H. S., and Zhang, X. F., 2016, "A Flexoelectric Double-Curvature Nonlinear Shell Energy Harvester," ASME J. Vib. Acoust., **138**(3), p. 031005.
[4] Huang, S. L., Chu, C. C., Chang, C. C., and Tzou, H. S., 2012, "Spatial Electrostrictive Actuation Characteristics of Flexible Circular Tubes," ASME J. Pressure Vessel Technol., **134**(2), p. 021201.
[5] Wang, D., Fan, M., Su, Z., and Tzou, H. S., 2019, "Frequency Control of Thin Plates With Light-Activated Shape-Memory Polymers," AIAA J., **57**(8), pp. 3579–3585.
[6] Hu, S. D., Li, H., and Tzou, H. S., 2015, ""Precision Microscopic Actuations of Parabolic Cylindrical Shell Reflectors," ASME Transactions," ASME J. Vib. Acoust., **137**(1), p. 011013.
[7] Jiang, J., Yue, H. H., Deng, Z. Q., and Tzou, H. S., 2013, "Cylindrical Shell Control With Center- and Corner-Placed Photostrictive Skew-Quad Actuator Systems,"," ASME J. Vib. Acoust., **134**(2), p. 024503.
[8] Wang, D., Fan, M., Su, Z., and Tzou, H. S., 2020, "Vibration Control of Hemispherical Shells With Light-Activated Shape Memory Polymers," AIAA J., **58**(3), pp. 1369–1376.
[9] Ginder, J. M., Nichols, M. E., Elie, L. D., and Clark, S. M., 2000, "Controllable-Stiffness Components Based on Magnetorheological Elastomers," Smart Structures and Materials 2000: Smart Structures and Integrated Systems, Newport Beach, CA.
[10] Lau, K. T., Zhou, L. M., and Tao, X. M., 2002, "Control of Natural Frequencies of a Clamped-Clamped Composite Beam With Embedded Shape Memory Alloy Wires," Compos. Struct., **58**(1), pp. 39–47.
[11] Wu, Y., Lin, Y., Zhou, Y., Zuo, F., Zheng, Z., and Ding, X., 2012, "Light-Induced Shape Memory Polymer Materials," Prog. Chem., **24**(10), pp. 2004–2010.
[12] Wang, S., Kaneko, D., and Kaneko, T., 2014, "Photo-Responsive Shape-Memory and Shape-Changing Polymers," Polym. Bull., **6**(1), pp. 89–98.
[13] Habault, D., Zhang, H. J., and Zhao, Y., 2013, "Light-Triggered Self-Healing and Shape-Memory Polymers," Chem. Soc. Rev., **42**(17), pp. 7244–7256.
[14] Lendlein, A., Jiang, H., Jünger, O., and Langer, R., 2005, "Light-Induced Shape-Memory Polymers," Nature, **434**(7035), pp. 879–882.
[15] Wu, L., Jin, C., and Sun, X., 2011, "Synthesis, Properties, and Light-Induced Shape Memory Effect of Multiblock Polyesterurethanes Containing Biodegradable Segments and Pendant Cinnamamide Groups," Biomacromolecules, **12**(1), pp. 235–241.
[16] Zhang, X., Zhou, Q., Liu, H., and Liu, H., 2014, "UV Light Induced Plasticization and Light Activated Shape Memory of Spiropyran Doped Ethylene-Vinyl Acetate Copolymers," Soft Matter, **10**(21), p. 3748.
[17] Iqbal, D., and Samiullah, M. H., 2013, "Photo-responsive Shape-Memory and Shape-Changing Liquid-Crystal Polymer Networks," Materials, **6**(1), pp. 116–142.
[18] Beblo, R. V., and Weiland, L. M., 2011, "Light Activated Shape Memory Polymer Characterization—Part II," ASME J. Appl. Mech., **78**(6), p. 061016.
[19] Li, H. Y., Li, H., and Tzou, H. S., 2015, "Frequency Control of Beams and Cylindrical Shells With Light-Activated Shape Memory Polymers," ASME J. Vib. Acoust., **137**(1), p. 011006.
[20] Li, H., Guo, D., and Tzou, H. S., 2017, "Responses of Rings with Light-Activated Shape Memory Polymers Regulated by Neural Network and Phase Shift," J. Intell. Mater. Syst. Struct., **28**(20), pp. 3079–3090.
[21] Sodhi, J. S., and Rao, I. J., 2010, "Modeling and Simulation of Light Activated Shape Memory Polymers," Int. J. Eng. Sci., **48**(11), pp. 1576–1589.
[22] Ma, J., Mu, X. M., Bowman, C. N., Sun, Y. Y., Dunn, M. L., Qi, H. J., and Fang, D. N., 2014, "A Photoviscoplastic Model for Photoactivated Covalent Adaptive Networks," J. Mech. Phys. Solids, **70**(1), pp. 84–103.
[23] Sodhi, J. S., Cruz, P. R., and Rao, I. J., 2015, "Inhomogeneous Deformations of Light Activated Shape Memory Polymers," Int. J. Eng. Sci., **89**(1), pp. 1–17.
[24] Akhmanov, S. A., and Nikitin, S. Y., 1997, *Physical Optics*, Oxford University Press, New York.
[25] Chen, L., Zhao, M., and Zhang, T., 2001, "The Testing Method of Mechanical Properties of Thin Films," J. Mech. Strength, **23**(4), pp. 413–429.
[26] GB/T1040.3-2006/ISO 527-3, 2006, "Plastics—Determination of Tensile Properties—Part, **3**. Test Conditions for Films and Sheets".
[27] Kim, W. G., 2008, "Photocure Properties of High-Heat-Resistant Photoreactive Polymers With Cinnamate Groups," J. Appl. Polym. Sci., **107**(6), pp. 3615–3624.